

## Gravitational Wave Consistency Relations for Multifield Inflation

Layne C. Price,<sup>1,\*</sup> Hiranya V. Peiris,<sup>2,†</sup> Jonathan Frazer,<sup>3,‡</sup> and Richard Easther<sup>1,§</sup>

<sup>1</sup>*Department of Physics, University of Auckland, Private Bag 92019 Auckland, New Zealand*

<sup>2</sup>*Department of Physics and Astronomy, University College London, London WC1E 6BT, United Kingdom*

<sup>3</sup>*Department of Theoretical Physics, University of the Basque Country UPV/EHU, 48040 Bilbao, Spain*  
(Received 15 September 2014; revised manuscript received 11 November 2014; published 22 January 2015)

We study the tensor spectral index  $n_t$  and the tensor-to-scalar ratio  $r$  in the simplest multifield extension to single-field, slow-roll inflation models. We show that multifield models with potentials  $V \sim \sum_i \lambda_i |\phi_i|^p$  have different predictions for  $n_t/r$  than single-field models, even when all the couplings are equal  $\lambda_i = \lambda_j$ , due to the probabilistic nature of the fields' initial values. We analyze well-motivated prior probabilities for the  $\lambda_i$  and initial conditions to make detailed predictions for the marginalized probability distribution of  $n_t/r$ . With  $\mathcal{O}(100)$  fields and  $p > 3/4$ , we find that  $n_t/r$  differs from the single-field result of  $n_t/r = -1/8$  at the  $5\sigma$  level. This gives a novel and testable prediction for the simplest multifield inflation models.

DOI: 10.1103/PhysRevLett.114.031301

PACS numbers: 98.80.Cq, 98.80.Es, 04.30.Db

A cosmological gravitational wave background (CGWB) is a compelling signature of inflation, which is already supported by the highly Gaussian primordial perturbations [1,2] and their broken scale invariance, now detected at  $5\sigma$  significance [3,4]. A large-amplitude CGWB provides fundamentally new tests of single-field slow-roll inflation via the consistency relation [5]  $n_t/r = -1/8$ , which relates the tensor spectral index  $n_t$  to the ratio of the tensor and scalar perturbation amplitudes  $r$ .

While there has been dramatic progress towards the direct detection of a CGWB through the  $B$ -mode polarization in the cosmic microwave background [6], measuring  $n_t$  is challenging with current technologies [7–9]. However, for  $r \gtrsim 0.1$  this will be feasible with the next generation of space-based [10,11], ground-based [12–15], and balloon-borne [16,17] experiments, while future 21 cm projects [18,19] could also detect lensing by a CGWB and direct detection experiments [20,21] would test the consistency condition using the lever arm between the cosmic microwave background and solar system scales to far greater accuracy with  $r \gtrsim \mathcal{O}(10^{-3})$ .

The simplest inflationary scenarios that yield an easily detectable CGWB are *monomial* models with the inflationary potential  $V \sim |\phi|^p$ , which have  $0.05 \lesssim r \lesssim 0.30$  for  $2/3 \lesssim p \lesssim 4$ . Single field models are *simple* but not necessarily *natural*, as many high energy theories yield large numbers of scalar degrees of freedom [22–25]. For multifield models the consistency relation is reduced to an inequality,  $n_t/r \leq -1/8$ . While  $r$  and  $n_t$  are correlated for  $N_f = 2$  [26,27], there is no known relationship between  $r$  and  $n_t$  when  $N_f$  is large.

In this Letter, we derive a robust prediction for  $n_t/r$  for  $N_f$ -monomial models, with potential

$$V = \frac{1}{p} \sum_i \lambda_i |\phi_i|^p, \quad (1)$$

where  $\lambda_i$  are real, positive constants and summations run over the number of fields,  $N_f$ . Equation (1) arises naturally in many high energy theories [28–35] and is a simple, intuitive generalization of the chaotic single-field slow-roll models.

We treat the  $\lambda_i$  and the values of  $\phi_i$  at a fixed number of  $e$ -folds before the end of inflation as independent random variables. When  $N_f \rightarrow \infty$ , the central limit theorem ensures that  $n_t/r$  is a Gaussian random variable. Critically,  $\langle n_t/r \rangle$  does not reduce to the single-field limit if the couplings are identical unless the field values  $\phi_{i,*}$  when the pivot scale  $k_*$  leaves the horizon are also fixed, except for the special case  $p = 2$ . The expected value of  $n_t/r$  depends only on two moments of the distributions of the  $\lambda_i$  and  $\phi_i$ , and is independent of  $N_f$ . The variance in  $n_t/r$  is  $s_{n_t/r}^2 \sim 1/N_f$  (for  $p > 3/4$ ), giving a sharp, generic prediction for the consistency relation in the many-field limit. This provides a direct test for distinguishing between  $N_f$ -monomial models and their single-field analogues.

*Model.*— In some cases the  $\lambda_i$  in Eq. (1) might be derivable from fundamental theory, but in general we are ignorant of their values, so we treat these terms as independent random variables (RVs) with a prior probability  $P(\lambda)$ . Similarly, we do not know the fields' initial conditions, so we also treat these as identically distributed, but possibly correlated, RVs with a prior probability  $P(\phi_0)$ . We then marginalize over the  $P(\lambda)$  and  $P(\phi_0)$  to produce a probability distribution for  $n_t/r$ . Since a change of variables  $\phi_i \rightarrow \tilde{\phi}_i(\phi_j, \lambda_j)$  will mix the  $\lambda_i$  and  $\phi_i$ , it is clear that there is no *a priori* difference between these two types of parameters, motivating our statistical approach.

The simplest choice for  $P(\phi_0)$  is a uniform distribution of  $\phi_{i,*}$  defined when the pivot scale  $k_*$  leaves the horizon  $N_* e$ -folds before the end of inflation. This choice contains the least Shannon information about the fields' initial states and ensures that most of the fields are dynamically

relevant. Further, this  $P(\phi_0)$  and others were extensively studied in Ref. [36], where it was shown that the initial conditions only weakly affect the predicted density spectra. The likely values of  $n_s$  and  $r$  for a related class of multifield monodromy models was derived in Ref. [37], finding  $0.955 \lesssim n_s \lesssim 0.975$ . Furthermore,  $r = 4p/N_*$ , and the non-Gaussianity is small.

*$\delta N$  formalism.*— The potential in Eq. (1) is sum-separable and, assuming slow roll,  $N_*$  is [38,39]

$$N_* = - \int_*^c \sum_i \frac{V_i}{V_i'} d\phi_i, \quad (2)$$

where  $V_i' = \lambda_i |\phi_i|^{p-1}$  and  $\phi_{i,*}$  and  $\phi_{i,c}$  denote field values at horizon crossing and the end of inflation, respectively. For  $N_f$ -monomial inflation

$$N_* = \frac{1}{2p} \sum_i [\phi_{i,*}^2 - \phi_{i,c}^2]. \quad (3)$$

The  $\delta N$  formalism relates the field perturbations at horizon crossing to the gauge-invariant curvature perturbation  $\zeta$  on constant density hypersurfaces via

$$\zeta \approx \sum_i N_{*,i} \delta\phi_{i,*}, \quad (4)$$

where  $N_{*,i} \equiv \partial N_*/\partial\phi_{i,*}$ . If the field perturbations are well approximated by a free field theory with power spectrum  $\mathcal{P}_{\delta\phi}^{ij} = (H_*/2\pi)^2 \delta^{ij}$  at horizon crossing, the tensor-to-scalar ratio is

$$r = \frac{8}{\sum_i N_{*,i} N_{*,i}}. \quad (5)$$

To first-order in slow-roll  $n_t = -2\epsilon$ , where

$$\epsilon = \frac{1}{2} \sum_i \left[ \frac{V_i'}{V} \right]^2. \quad (6)$$

For  $N_f$ -monomial models, the field values  $\phi_{i,c}$  at the end of inflation can typically be neglected. This horizon crossing approximation (HCA) (e.g., Refs. [38,40]) is a simplification of the  $\delta N$  formalism that incorporates the superhorizon evolution of  $\zeta$ , but ignores quantities contributing to  $N_*$  from the end-of-inflation surface. Setting  $\phi_{i,c} \rightarrow 0$  in Eq. (3), we find

$$\frac{n_t}{r} = -\frac{1}{4p^2} \epsilon \sum_i \phi_{i,*}^2, \quad (7)$$

where we restrict our attention to cases that are slowly rolling at horizon crossing. Requiring  $\epsilon \lesssim 0.1$  then sets the maximum deviation from the single-field result as

$$-\left(\frac{N_*}{2p}\right) \times \mathcal{O}(10^{-1}) \lesssim \frac{n_t}{r} \leq -\frac{1}{8}. \quad (8)$$

*The many-field limit.*— We build the probability distribution for  $n_t/r$  by marginalizing Eq. (7) over  $P(\phi_0)$  and  $P(\lambda)$  and use the central limit theorem (CLT) to take the large  $N_f$  limit,  $N_f \rightarrow \infty$ . By Eq. (3) the HCA implies that  $P(\phi_0)$  is a uniform distribution pulled back onto an  $N_f$ -sphere in field space with radius  $\sqrt{2pN_*}$ . Since the multivariate normal distribution  $\vec{x} \sim \mathcal{N}(0, \mathbb{1})$  is invariant under rotations of  $\vec{x}$ , we can sample this  $N_f$ -sphere uniformly by defining

$$\phi_{i,*} = \sqrt{\frac{2pN_*}{\sum_j x_j^2}} x_i \quad \text{for } \vec{x} \sim \mathcal{N}(0, \mathbb{1}). \quad (9)$$

Using Eq. (9), the summations in Eqs. (6) and (7) are

$$\sum_i \lambda_i^n |\phi_{i,*}|^m = \sum_i \lambda_i^n \left[ \frac{2pN_*}{\sum_j x_j^2} \right]^{(m/2)} |x_i|^m. \quad (10)$$

As  $N_f \rightarrow \infty$  the CLT shows that the numerator is normally distributed with mean

$$\mu_{\text{num}} = N_f (2pN_*)^{m/2} \langle \lambda^n \rangle \langle |x|^m \rangle \quad (11)$$

and standard deviation

$$s_{\text{num}} = \sqrt{N_f} (2pN_*)^{m/2} \sigma_{n,m}, \quad (12)$$

where  $\langle \cdot \rangle$  indicates expected value and

$$\sigma_{n,m}^2 \equiv \langle \lambda^{2n} \rangle \langle |x|^{2m} \rangle - \langle \lambda^n \rangle^2 \langle |x|^m \rangle^2, \quad (13)$$

which assumes that the  $\lambda_i$  and  $x_j$  are independent. Finally, the denominator in Eq. (9) is drawn from the  $\chi$ -distribution, which is closely approximated by  $\mathcal{N}(\sqrt{N_f}, 1/\sqrt{2})$  for  $x_i \sim \mathcal{N}(0, 1)$ .

The numerator and denominator in Eq. (10) are correlated by the constraint in Eq. (3). For a given variance in  $P(\lambda)$ , the correlation  $\gamma$  is maximized when  $m = 2$  and  $|\gamma| \rightarrow 1$  as the variance vanishes. Since each  $\sum_i \lambda_i^n |\phi_{i,*}|^m$  is uniquely determined given  $\vec{\lambda}$  and  $\vec{\phi}_*$ , we expect a strong correlation between the numerator and denominator in Eq. (6) for typical choices of  $P(\lambda)$ . This significantly reduces the variance of  $n_t/r$ , and ensures a sharp prediction for its value. We numerically calculate  $\gamma$  after defining the priors on  $\lambda$ .

For any normally distributed variable  $y \sim \mathcal{N}(\mu, \sigma)$

$$\langle |y|^m \rangle = \frac{2^{(m/2)} \sigma^m}{\sqrt{\pi}} \Gamma\left(\frac{1+m}{2}\right) F_{1,1}\left(\frac{-m}{2}; \frac{1}{2}; \frac{-\mu^2}{2\sigma^2}\right), \quad (14)$$

for  $m > -1$ , and  $F_{1,1}$  is the confluent hypergeometric function of the first kind. If  $\mu = 0$ , as for  $x_i \sim \mathcal{N}(0, 1)$ , then  $F_{1,1} = 1$  and only the  $\Gamma$  function contributes to the moments.

If  $m < -1$ ,  $\langle |y|^m \rangle$  may diverge if  $P(y = 0)$  does not vanish fast enough. This is indeed the case for  $x_i \sim \mathcal{N}(0, 1)$ , and we cannot predict the distribution of the sums in Eq. (10) with  $m \leq -1$ . Sums like Eq. (10) are effectively finite numerical approximations to the integral

$$\frac{1}{N_f} \sum_i \lambda_i^n |x_i|^m \approx \int |x|^m \mathcal{N}(0, 1) dx \int \lambda^n P(\lambda) d\lambda, \quad (15)$$

which diverges for  $m < -1$ . While ratios of these sums might be well defined [41], our approach shows that a finite prediction for both the mean and the standard deviation of  $n_t/r$  requires  $p > 3/4$ , while only requiring a finite mean needs  $p > 1/2$ , using the CLT.

*The method.*— Since  $n_t/r$  is given by Eq. (7) and the sums in Eq. (10) are ratios of correlated, normally distributed RVs, the key tool for this analysis is the ratio distribution  $f_{\text{ratio}}(\alpha/\beta)$  for normally distributed RVs  $\alpha$  and  $\beta$ . If  $w \equiv \alpha/\beta$ , then as  $P(\beta > 0) \rightarrow 1$  the CDF for the ratio distribution  $f_{\text{ratio}}(w)$  is approximately [42]

$$F_{\text{ratio}}(w) = \Phi \left[ \frac{\mu_\beta w - \mu_\alpha}{\sigma_\alpha \sigma_\beta a(w)} \right], \quad (16)$$

where  $\mu_i$  and  $\sigma_i^2$  are the respective means and variances,

$$a(w) \equiv \left[ \frac{w^2}{\sigma_\alpha^2} - \frac{2\gamma w}{\sigma_\alpha \sigma_\beta} + \frac{1}{\sigma_\beta^2} \right]^{1/2}, \quad (17)$$

and

$$\Phi(z) \equiv \frac{1}{2} \left[ 1 + \text{Erf} \left( \frac{z}{\sqrt{2}} \right) \right] \quad (18)$$

for real  $z$ . When  $N_f$  is large, the  $f_{\text{ratio}}$  approaches a normal distribution with mean  $\mu_\alpha/\mu_\beta$  and standard deviation

$$s = \frac{\sqrt{\mu_\beta^2 \sigma_\alpha^2 - 2\gamma \mu_\alpha \mu_\beta \sigma_\alpha \sigma_\beta + \mu_\alpha^2 \sigma_\beta^2}}{\mu_\beta^2}. \quad (19)$$

The mean of the  $f_{\text{ratio}}$  is independent of the correlations  $\gamma$ , and the standard deviation for  $n_t/r$  is a straightforward—but messy—algebraic function of  $\langle \lambda \rangle$ ,  $\langle \lambda^2 \rangle$ , and  $\langle \lambda^4 \rangle$ , as well as  $\langle |x|^m \rangle$  for  $m = 2, 4, p, 2p, 2p - 2$ , and  $4p - 4$ .

To obtain the distribution  $f_{\text{ratio}}(n_t/r)$  we express the consistency relation in terms of the sums in Eq. (10) as

$$\frac{n_t}{r} = -\frac{pN_*}{4} \frac{\left[ \sum_i \lambda_i^2 |\phi_{i,*}|^{2p-2} \right]}{\left[ \left( \sum_j \lambda_j |\phi_j|^p \right)^2 \right]}. \quad (20)$$

For each sum above, we calculate the covariance in Eq. (10) between the numerator and denominator given  $P(\lambda)$ , and use Eq. (19) to find the variance of the sum. Although the denominator  $(\sum_i \lambda_i |\phi_{i,*}|^p)^2$  is then  $\chi^2$  distributed, this is approximately normal in the many-field limit. We then substitute these two normally distributed RVs back into Eq. (16). Similarly, we evaluate the correlation between the numerator and denominator in Eq. (20), finally obtaining the probability distribution for  $n_t/r$ .

*Novel multifield predictions.*— From the ratio distribution (16), as  $N_f \rightarrow \infty$  the value of  $n_t/r$  in Eq. (20) is normally distributed with a mean

$$\left\langle \frac{n_t}{r} \right\rangle_{N_f \uparrow} = \left[ -\frac{1}{8} \right] \frac{\langle \lambda^2 \rangle}{\langle \lambda \rangle^2} \left[ \frac{\sqrt{\pi} \Gamma(p - \frac{1}{2})}{2\Gamma^2(\frac{p+1}{2})} \right] \quad (21)$$

and a standard deviation proportional to

$$s_{n_t/r} \propto \frac{1}{\sqrt{N_f}} \rightarrow 0 \quad \text{as } N_f \rightarrow \infty, \quad (22)$$

which can be found by substituting the means, variances, and correlations of Eq. (10) into Eq. (19).

The first bracketed term in Eq. (21) is the single-field prediction, the second is due to the couplings  $\lambda_i$ , and the third arises from the uniform prior for  $\phi_{i,*}$  on the horizon-crossing surface. This last term is due only to the spread in the field values at horizon crossing and is independent of everything except  $p$ . The functional form of this term is fixed by the uniform prior distribution on the horizon crossing surface, but other prior probabilities for  $\phi_{i,*}$  result in qualitatively similar behavior as demonstrated in Ref. [36]. As Eq. (22) vanishes in the many-field limit, Eq. (21) is the generic multifield prediction, which deviates from the single-field result at  $> 5\sigma$  for  $N_f \gtrsim \mathcal{O}(10^2)$  for typical  $P(\lambda)$ .

Consequently, even if  $\langle \lambda^2 \rangle = \langle \lambda \rangle^2$ ,  $N_f$ -monomial models do not predict  $n_t/r = -1/8$ , unless the  $\phi_{i,*}$  are also identical. Figure 1 compares the predicted value for

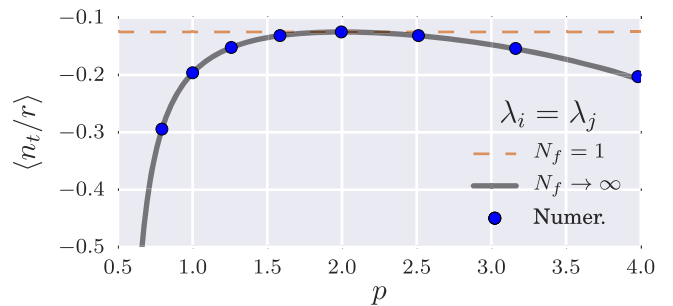


FIG. 1 (color online). The multifield prediction from Eq. (21) compared to the numerical mean  $\langle n_t/r \rangle$  of simulations with 5000 samples, at each plotted value of  $p$ , with  $N_f = 1000$  using the horizon-crossing approximation. The field values  $\phi_{i,*}$  as the pivot scale  $k_*$  leaves the horizon are drawn from a uniform prior on the surface in Eq. (3) and all the couplings  $\lambda_i$  are identical.

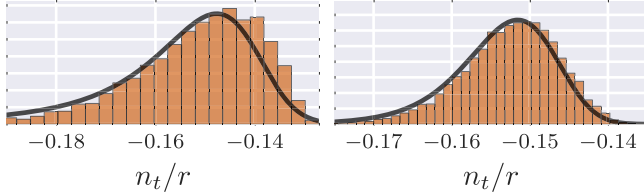


FIG. 2 (color online). Predicted probability distributions for  $n_t/r$  with  $p = 2$  compared with histograms built from 10 000 numerical samples. The couplings  $\lambda_i$  are drawn from the uniform model with (left)  $N_f = 20$  and (right)  $N_f = 100$ . For  $N_f \lesssim \mathcal{O}(10^2)$ , the distribution is skewed toward positive values as predicted.

$\langle n_t/r \rangle$  in Eq. (21), with all  $\lambda_i$  equal, to numerical results obtained by directly evaluating  $n_t/r$  with Eq. (7), showing excellent agreement for many fields. The divergence at  $p = 1/2$  reflects the fact that  $\langle |x|^{2p-2} \rangle \rightarrow \infty$ . Thus, when  $p \leq 1/2$ ,  $\langle n_t/r \rangle$  may be arbitrarily large, which violates the slow-roll assumption. Consequently, these models are most easily distinguished from their single field analogues, but the hardest to make accurate predictions for.

*Specific examples.*— To understand how the mean  $\langle n_t/r \rangle$  in Eq. (21) is affected by  $P(\lambda)$  we compare two explicit priors that are widely used in Bayesian analyses of inflation [4,43–46]. We focus on the  $p = 2$  case, since the dependence on the prior on  $\phi_{i,*}$  in Eq. (21) cancels for this scenario.

We look at two cases: uniform prior probabilities over  $\lambda_i$  or  $\alpha_i$  for  $\lambda_i \equiv 10^{\alpha_i}$ , which we denote the uniform model and log model, respectively. The uniform model would be applicable when the relevant scale of  $\lambda_i$  is known to within an order of magnitude, while the log model effectively scans over a range of physical scales.

For the uniform model, the  $\lambda_i$  are drawn from  $\mathcal{U}[a, b]$ , and Eq. (21) becomes

$$\left(\frac{n_t}{r}\right)_{p=2}^{\text{unif}} = -\frac{1}{6} \left[ \frac{b^2 + ab + a^2}{(b+a)^2} \right]. \quad (23)$$

For  $\lambda_i \in [10^{-14}, 10^{-13}]$ , as  $N_f \rightarrow \infty$  the predicted correlation coefficient for  $f_{\text{ratio}}(n_t/r)$  is  $\gamma \approx -0.98$  and  $\langle n_t/r \rangle = -0.153$ . We plot  $f_{\text{ratio}}$  and the results of 10 000 numerical realizations using the HCA in Fig. 2. We find excellent agreement with Eq. (23), with  $f_{\text{ratio}}$  accurately capturing the higher order moments of the  $n_t/r$  distribution for  $N_f \gtrsim 20$ . For  $p = \{3/2, 2, 3\}$  the single-field result  $n_t/r = -1/8$  is a  $5\sigma$  deviation from the mean in Eq. (23) for  $N_f \gtrsim \{120, 120, 200\}$ , respectively.

For the log model with  $\alpha \sim \mathcal{U}[a, b]$ ,

$$\left(\frac{n_t}{r}\right)_{p=2}^{\text{log}} = -\frac{\log(10)(b-a)}{16} \left[ \frac{10^b + 10^a}{10^b - 10^a} \right]. \quad (24)$$

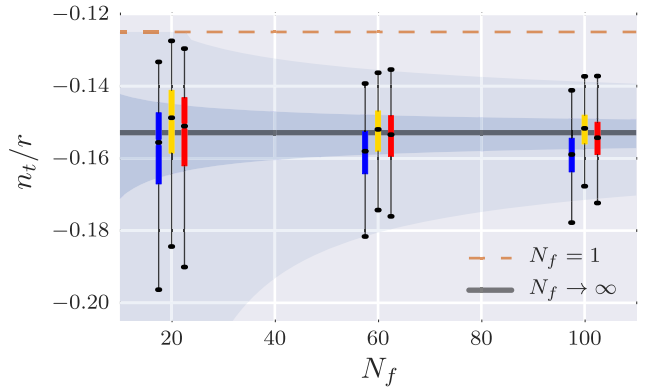


FIG. 3 (color online). The consistency relation for the uniform model with  $p = 2$  is plotted for different  $N_f$ , marginalizing over initial field values. The boxes (whiskers) cover the 50%(97%) CIs and the gray regions delineate the same ranges as predicted by the HCA and the central limit theorem. The (dashed) brown and (solid) gray lines are the single-field and the many-field HCA predictions, respectively. For each case we present results derived from full numerical solutions to the mode equations [blue (left)], the slow-roll prediction using the HCA [yellow (center)], and the slow-roll prediction including the end-of-inflation surface [red (right)] for  $N_f = 20, 60$ , and  $100$ .

If  $a \rightarrow b$ , we recover the single-field result in both Eqs. (23) and (24). However, Eq. (24) diverges as  $a \rightarrow -\infty$ , reflecting the failure of slow roll in the limit of widely separated scales. For  $\alpha \in [-14, -12]$  the log model predicts  $\mathcal{P}_\zeta \sim \mathcal{O}(10^{-9})$ ,  $\epsilon \lesssim 0.03$ ,  $\gamma \approx -0.95$ , and  $n_t/r = -0.294$ . For  $p = \{3/2, 2, 3\}$  the single-field result is a  $5\sigma$  deviation from the mean in Eq. (24) for  $N_f \gtrsim \{145, 135, 255\}$ , respectively.

*Relaxing the approximations.*— Fig. 3 compares the HCA prediction to numerical results that include the contribution from the end-of-inflation surface in Eq. (3), with  $\phi_{i,c} \neq 0$ . We numerically solve the background Klein-Gordon equations for 1000 realizations, finding the field values at the end of inflation (defined by  $\epsilon = 1$ ) and obtaining the full  $\delta N$  prediction without using the HCA. Figure 3 also incorporates both the subhorizon evolution of the modes and any non-slow-roll behavior by solving the mode equations numerically, as in Refs. [36,47], using the MULTIMODECODE [48]. Results are plotted for the uniform model, with the ranges  $\lambda_i \in [10^{-14}, 10^{-13}]$  and  $p = 2$ .

In all cases the numerical results are well-approximated by the HCA. The HCA results are marginally larger than the numerical results, which we attribute to second-order corrections to the slow-roll equations;  $n_t = -2\epsilon/(1-\epsilon)$ , which suppresses  $n_t$  relative to the first-order approximation. The variances in the numerical results scale as  $\sigma^2 \propto 1/\sqrt{N_f}$ , as predicted by the HCA results, confirming that many-field models make sharp predictions for  $n_t/r$ .

*Conclusion.*— We have computed the probability distribution for the consistency relation  $n_t/r$  for inflation driven by multiple scalar fields with monomial potential

terms, as a function of the distribution of couplings and initial field values. The single-field result is clearly distinguishable from the many-field limit, providing a clean and compelling signature that distinguishes these models from their single-field analogues. Other than for the quadratic case, this result holds even when the couplings are identical.

We focused on computing the slow roll parameter  $\epsilon$ , but the nature of the slow-roll hierarchy [49] indicates that this approach will generalize to a variety of observables, so quantities such as  $f_{\text{NL}}$  that rely on the second and higher slow-roll parameters should also have precise predictions that deviate from the single-field expectation even when the couplings are degenerate. This provides a further compelling example of a multifield scenario in which the observables have a sharp and *generic* prediction in the many-field limit [32,34–36,40,41,50–57].

The expected value  $\langle n_t/r \rangle$  depends on only two moments of the prior probability distributions  $P(\lambda)$  and  $P(\phi_0)$ , and the corresponding variance is  $s_{n_t/r}^2 \propto 1/N_f$ . The single-field expectation of  $n_t/r = -1/8$  differs from the multifield result at the  $5\sigma$  level when  $N_f \gtrsim \mathcal{O}(10^2)$ . Consequently, given specific priors for the field values and couplings, we obtain generic and testable predictions for the consistency relations in this large and interesting class of multifield inflation models.

We thank Grigor Aslanyan, Andrew Jaffe, and Jonathan White for helpful discussions. H. V. P. is supported by STFC and the European Research Council under the European Community’s Seventh Framework Programme (FP7/2007-2013) / ERC Grant Agreement No. 306478-CosmicDawn. J. F. is supported by IKERBASQUE, the Basque Foundation for Science. We acknowledge the contribution of the NeSI high-performance computing facilities. New Zealand’s national facilities are provided by the New Zealand eScience Infrastructure (NeSI) and funded jointly by NeSI’s collaborator institutions and through the Ministry of Business, Innovation & Employment’s Research Infrastructure programme [58]. This work has been facilitated by the Royal Society under their International Exchanges Scheme. This work was supported in part by National Science Foundation Grant No. PHYS-1066293 and the hospitality of the Aspen Center for Physics.

\*lpri691@aucklanduni.ac.nz

<sup>†</sup>h.peiris@ucl.ac.uk

<sup>‡</sup>j.frazer@ucl.ac.uk

<sup>§</sup>r.easther@auckland.ac.nz

- [1] P. Ade *et al.* (Planck Collaboration), *Astron. Astrophys.* **571**, A24 (2014).  
 [2] B. Leistedt, H. V. Peiris, and N. Roth, *Phys. Rev. Lett.* **113**, 221301 (2014).

- [3] P. Ade *et al.* (Planck Collaboration), *Astron. Astrophys.* **571**, A16 (2014).  
 [4] P. Ade *et al.* (Planck Collaboration), *Astron. Astrophys.* **571**, A22 (2014).  
 [5] E. J. Copeland, E. W. Kolb, A. R. Liddle, and J. E. Lidsey, *Phys. Rev. Lett.* **71**, 219 (1993).  
 [6] P. Ade *et al.* (BICEP2 Collaboration), *Phys. Rev. Lett.* **112**, 241101 (2014).  
 [7] L. Verde, H. Peiris, and R. Jimenez, *J. Cosmol. Astropart. Phys.* **01** (2006) 019.  
 [8] S. Dodelson, *Phys. Rev. Lett.* **112**, 191301 (2014).  
 [9] J. Caligiuri and A. Kosowsky, *Phys. Rev. Lett.* **112**, 191302 (2014).  
 [10] D. Baumann *et al.* (CMBPol Study Team), *AIP Conf. Proc.* **1141**, 10 (2009).  
 [11] P. Andre *et al.* (PRISM Collaboration), arXiv:1306.2259.  
 [12] R. W. Ogburn *et al.*, *Proc. SPIE Int. Soc. Opt. Eng.* **8452**, 1A (2012).  
 [13] Z. Ahmed *et al.*, *Proc. SPIE Int. Soc. Opt. Eng.* **9153**, 91531N (2014).  
 [14] T. Matsumura *et al.*, *Proc. SPIE Int. Soc. Opt. Eng.* **8452**, 84523E (2012).  
 [15] B. A. Benson *et al.*, *Proc. SPIE Int. Soc. Opt. Eng.* **9153**, 91531P (2014).  
 [16] P. Oxley *et al.*, *Proc. SPIE Int. Soc. Opt. Eng.* **5543**, 320 (2004).  
 [17] B. Crill *et al.*, *Proc. SPIE Int. Soc. Opt. Eng.* **7010**, 70102P (2008).  
 [18] K. W. Masui and U.-L. Pen, *Phys. Rev. Lett.* **105**, 161302 (2010).  
 [19] L. Book, M. Kamionkowski, and F. Schmidt, *Phys. Rev. Lett.* **108**, 211301 (2012).  
 [20] T. L. Smith, H. V. Peiris, and A. Cooray, *Phys. Rev. D* **73**, 123503 (2006).  
 [21] L. Boyle, K. M. Smith, C. Dvorkin, and N. Turok, arXiv:1408.3129.  
 [22] M. Grana, *Phys. Rep.* **423**, 91 (2006).  
 [23] M. R. Douglas and S. Kachru, *Rev. Mod. Phys.* **79**, 733 (2007).  
 [24] F. Denef, M. R. Douglas, and S. Kachru, *Annu. Rev. Nucl. Part. Sci.* **57**, 119 (2007).  
 [25] F. Denef, arXiv:0803.1194.  
 [26] N. Bartolo, S. Matarrese, and A. Riotto, *Phys. Rev. D* **64**, 123504 (2001).  
 [27] D. Wands, N. Bartolo, S. Matarrese, and A. Riotto, *Phys. Rev. D* **66**, 043520 (2002).  
 [28] A. R. Liddle, A. Mazumdar, and F. E. Schunck, *Phys. Rev. D* **58**, 061301 (1998).  
 [29] P. Kanti and K. A. Olive, *Phys. Rev. D* **60**, 043502 (1999).  
 [30] P. Kanti and K. A. Olive, *Phys. Lett. B* **464**, 192 (1999).  
 [31] N. Kaloper and A. R. Liddle, *Phys. Rev. D* **61**, 123513 (2000).  
 [32] R. Easther and L. McAllister, *J. Cosmol. Astropart. Phys.* **05** (2006) 018.  
 [33] S. Dimopoulos, S. Kachru, J. McGreevy, and J. G. Wacker, *J. Cosmol. Astropart. Phys.* **08** (2008) 003.  
 [34] S. A. Kim and A. R. Liddle, *Phys. Rev. D* **74**, 023513 (2006).  
 [35] S. A. Kim and A. R. Liddle, *Phys. Rev. D* **76**, 063515 (2007).

- [36] R. Easther, J. Frazer, H. V. Peiris, and L. C. Price, *Phys. Rev. Lett.* **112**, 161302 (2014).
- [37] D. Wenren, [arXiv:1405.1411](https://arxiv.org/abs/1405.1411).
- [38] F. Vernizzi and D. Wands, *J. Cosmol. Astropart. Phys.* **05** (2006) 019.
- [39] T. Battefeld and R. Easther, *J. Cosmol. Astropart. Phys.* **03** (2007) 020.
- [40] S. A. Kim and A. R. Liddle, *Phys. Rev. D* **74**, 063522 (2006).
- [41] J. Frazer, *J. Cosmol. Astropart. Phys.* **01** (2014) 028.
- [42] D. V. Hinkley, *Biometrika* **56**, 635 (1969).
- [43] M. J. Mortonson, H. V. Peiris, and R. Easther, *Phys. Rev. D* **83**, 043505 (2011).
- [44] J. Martin, C. Ringeval, and R. Trotta, *Phys. Rev. D* **83**, 063524 (2011).
- [45] R. Easther and H. V. Peiris, *Phys. Rev. D* **85**, 103533 (2012).
- [46] J. Martin, C. Ringeval, R. Trotta, and V. Vennin, *J. Cosmol. Astropart. Phys.* **03** (2014) 039.
- [47] D. Salopek, J. Bond, and J. M. Bardeen, *Phys. Rev. D* **40**, 1753 (1989).
- [48] L. C. Price, J. Frazer, J. Xu, H. V. Peiris, and R. Easther, [arXiv:1410.0685](https://arxiv.org/abs/1410.0685).
- [49] R. Easther and J. T. Giblin, *Phys. Rev. D* **72**, 103505 (2005).
- [50] A. Aazami and R. Easther, *J. Cosmol. Astropart. Phys.* **03** (2006) 013.
- [51] L. Alabidi and D. H. Lyth, *J. Cosmol. Astropart. Phys.* **05** (2006) 016.
- [52] Y.-S. Piao, *Phys. Rev. D* **74**, 047302 (2006).
- [53] D. I. Kaiser and E. I. Sfakianakis, *Phys. Rev. Lett.* **112**, 011302 (2014).
- [54] R. Kallosh and A. Linde, *J. Cosmol. Astropart. Phys.* **07** (2013) 002.
- [55] R. Kallosh and A. Linde, *J. Cosmol. Astropart. Phys.* **10** (2013) 033.
- [56] R. Kallosh and A. Linde, *J. Cosmol. Astropart. Phys.* **12** (2013) 006.
- [57] D. Sloan, [arXiv:1407.3977](https://arxiv.org/abs/1407.3977).
- [58] <http://www.nesi.org.nz>.